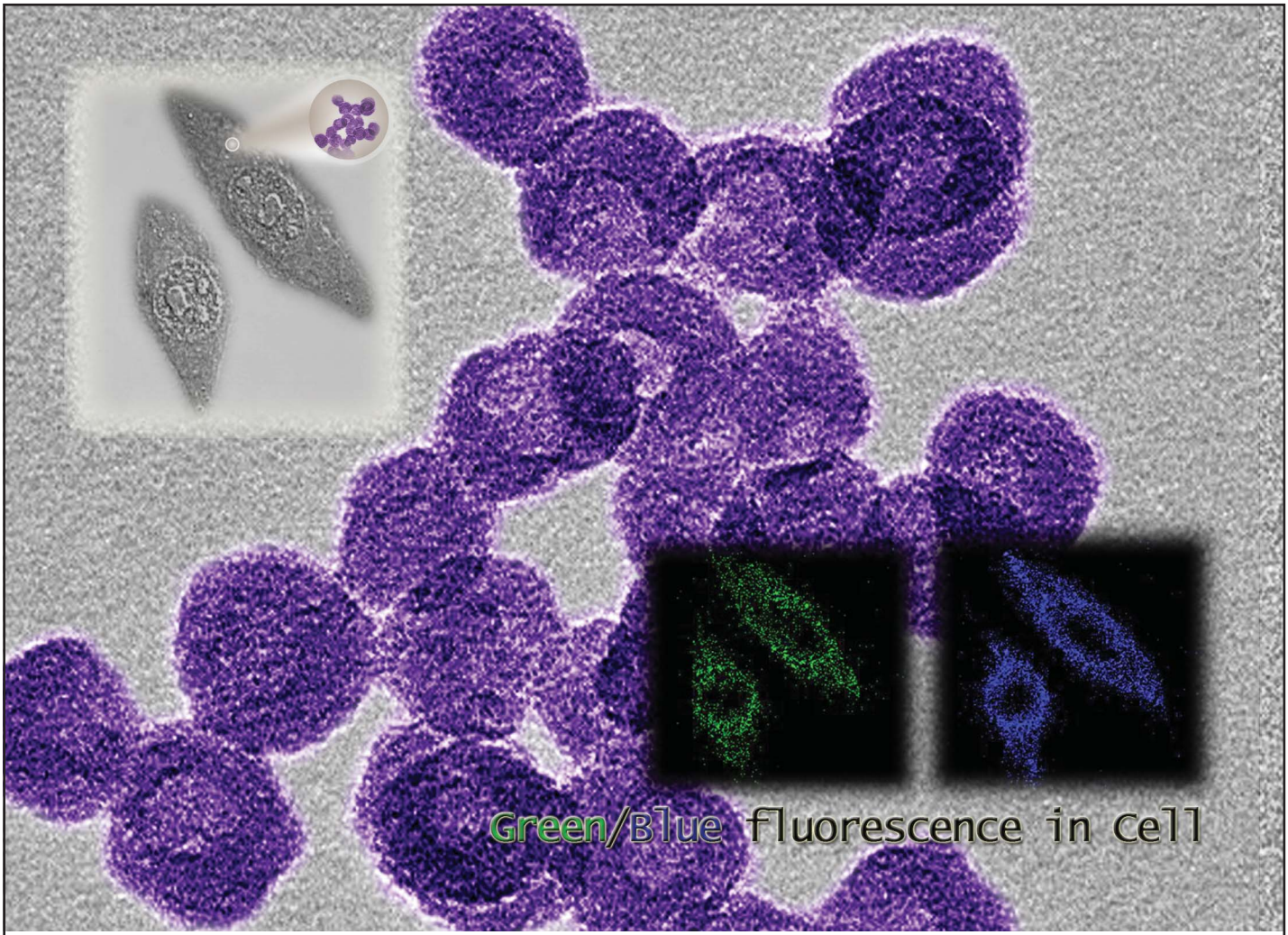

Showcasing research from the Department of Chemistry and Nano Science, Ewha Womans University, Seoul, South Korea.

Title: Photoluminescent nano graphitic/nitrogen-doped graphitic hollow shells as a potential candidate for biological applications

Water-dispersible nanosized graphitic/N-doped graphitic hollow spheres were successfully synthesized using a soft chemical route. Cellular uptake of the graphitic/N-doped graphitic hollow spheres was evaluated in human HeLa cells, demonstrating its main localization in the cytoplasm, and blue and green fluorescence signals were observed with low toxicity in the cells.

As featured in:

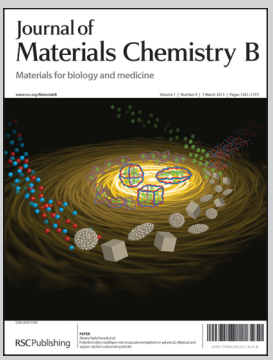

See J.-E. Park *et al.*, *J. Mater. Chem. B*, 2013, **1**, 1229.

RSC Publishing

www.rsc.org/MaterialsB

Registered Charity Number 207890

Journal of Materials Chemistry B

RSC Publishing

PAPER

Cite this: J. Mater. Chem. B, 2013, 1, 1229

Photoluminescent nanographitic/nitrogen-doped graphitic hollow shells as a potential candidate for biological applications†

Ji-eun Park,[a] Ekaterina D. Grayfer,[ae] Yeongri Jung,[a] Kyung Kim,[a] Kang-Kyun Wang,[b] Yong-Rok Kim,[b] Duhee Yoon,[c] Hyeonsik Cheong,[c] Hae-Eun Chung,[d] Soo-Jin Choi,[d] Jin-Ho Choy[a] and Sung-Jin Kim*[a]

Received 6th October 2012
Accepted 7th January 2013

DOI: 10.1039/c2tb00210h

www.rsc.org/MaterialsB

Water-dispersible graphitic hollow spheres were synthesized using a soft chemical route under hydrothermal conditions by glucose carbonization using a magnetite/silica-encapsulated core–shell sphere as a template. Carbonization on the templates happens as the magnetite core is partially or completely eliminated depending on the reaction conditions. Therefore, nano-sized graphitic hollow spheres or magnetite-core-encapsulated graphitic shells could be obtained. Also nitrogen-doped graphitic spheres were synthesized by a hydrothermal reaction. The graphitic and nitrogen-doped graphitic spheres show wavelength dependent photoluminescence in 300–600 nm range. The photoluminescence seems to depend on the fraction of the sp^2 domains and N-doping, therefore, tunable PL emission can be achieved by controlling the nature of sp^2 sites. In addition the cellular uptake of the graphitic hollow spheres was evaluated in human HeLa cells, demonstrating its main localization in the cytoplasm. A blue fluorescence signal was the most intensively observed in the cellular uptake process, although some green and red fluorescence was also observed. Since the cores of Fe_3O_4 could be completely or partly eliminated in a controllable way, it can be used as a magnetic resonance imaging agent. In addition, their easily modifiable hydrophilic surfaces for multi-functionality and hydrophobic voids covered by oxidized graphite make them promising candidates for applications in cellular photo-imaging and targeted drug delivery.

Introduction

Nano-structured carbon based materials have received much attention recently because their physical properties could make them very useful in many areas of science and technology. However, the difficulty of manipulating as-produced carbon-based nanomaterials greatly limits their use in solvents. Water dispersibility is one of the desired properties of the carbonaceous materials.

In view of the water dispersible properties, nano-sized graphitic oxide has received great interest among graphitic materials. Previously, there have been reports of fabrication of hollow carbon nano-structures[1–7] or nanoparticle-encapsulated carbon nano-structures.[8–11]

Recently, luminescence properties of graphene oxide have been reported,[12,13] and it is predicted to be promising for applications in bionanotechnology such as chemo/biosensing and cell imaging.[14,15] In terms of the biological application of nano-structured carbon materials, Zhao *et al.* prepared fluorescent carbon nanocrystals[16] by electrooxidation of a graphite column electrode which showed low cytotoxicity of carbon nanocrystals in 293T human kidney cells. Yu *et al.* obtained nanodiamonds with a nontoxic nature and different emission colors.[17] These reports provided the possibility of biological use of nano-structured carbon materials. However, intensive investigations of hollow or nanoparticle-encapsulated carbon nano-structures with photoluminescence (PL) properties are still lacking. Also nitrogen-doped graphene (N-graphene) shows different properties compared with the pristine graphene and graphene oxide. Due to its unique physical and chemical properties, N-graphene has been extensively used in various fields such as biosensing,[18] high-performance ultracapacitors,[19] lithium batteries,[20] fuel cells and electrocatalysis.[21]

We report the preparation and spectroscopic characterization of graphitic hollow spheres (GHS) with an empty space or

[a]Department of Chemistry and Nanoscience, Ewha Womans University, Seoul 120-750, Korea. E-mail: sjkim@ewha.ac.kr; Fax: +82-2-3277-3419
[b]Department of Chemistry, Yonsei University, Seoul 120-749, Korea
[c]Department of Physics, Sogang University, Seoul 121-742, Korea
[d]Department of Food Science and Technology, Seoul Women's University, Seoul 139-774, Korea
[e]Nikolaev Institute of Inorganic Chemistry, Russian Academy of Sciences, Acad. Lavrentiev prosp. 3, Novosibirsk, 630090, Russia

† Electronic supplementary information (ESI) available. See DOI: 10.1039/c2tb00210h

with magnetite core inside. In this report, we synthesized non-aggregated and water-dispersible GHS with fluorescence at mild condition. To investigate PL properties of GHS, we also prepared nitrogen-doped GHS (N-GHS) and demonstrated the wide range of PL wavelength. Finally, we report a cellular uptake process study of GHS. However, to the best of our knowledge, no studies have been reported yet to investigate the cytotoxicity of hollow carbon nano-structures. Here in, we carry out cellular uptake experiments on the fluorescent GHS and N-GHS in human HeLa cells. The controllable nano-size, hydrophilicity, nontoxicity and photoluminescence of GHS and N-GHS make them enormously useful for applications in the biomedical field such as cellular imaging, therapeutics, biosensing and fluorescence tags.

Experimental details

Synthesis

Magnetite (Fe_3O_4) nanoparticles (NPs) (1): mono-dispersed magnetite NPs were prepared from an iron oleate precursor as reported elsewhere.[22] For the formation of Fe_3O_4 NPs, 40 mmol of dried iron oleate complex and 20 mmol of oleic acid were dissolved in 200 g of 1-octadecene. The temperature was increased to 320 °C, and held for 30 min. The resulting solution was washed with excess acetone and collected by centrifugation.

Magnetite@silica-encapsulated core–shell spheres (Fe_3O_4@SiO_2) (2): the silica-coated magnetite NPs were prepared by the water-in-oil micro-emulsion technique. For a typical synthesis, Fe_3O_4 NPs (1) pre-dispersed in cyclohexane was injected into 8 mL of Igepal CO-520 in 200 mL of cyclohexane. Next, 1.3 mL of 30% NH_4OH solution was added with stirring and then 3 mL of TEOS were added. The mixture was stirred for 12 h at room temperature. The resulting dark brown silica-coated NPs were washed with ethanol and centrifuged.

Silica@graphitic hollow spheres (SiO_2@GHS) (3) or magnetite@silica@graphitic hollow spheres (Fe_3O_4@SiO_2@GHS): Fe_3O_4@SiO_2 (2) pre-dispersed in an aqueous glucose solution were transferred into a Teflon lined stainless steel autoclave. The temperature was increased to 180 °C and maintained for 4–16 h. After the reaction went to completion, the reactor was rapidly cooled with cold tap water. The resulting upper bright-yellow solution containing SiO_2@GHS NPs was separated from solution and dried under vacuum.

Graphitic hollow spheres (GHS) (4) or magnetite encapsulated graphitic hollow spheres (Fe_3O_4@GHS): the dried SiO_2@GHS (3) or Fe_3O_4@SiO_2@GHS were transferred to a polyethylene bath of 7 M HF solution and stored to allow chemical etching to remove SiO_2 and undesired impurities. A yellowish-brown powder floating on the surface of the HF solution was obtained and washed with water.

Nitrogen-doped graphitic hollow spheres (N-GHS) (5): for preparation of N-GHS, 30% ammonia was added to 70 mL of the described GHS (4) solution to adjust the pH value to 10, then 1 mL of triethylamine (TEA) was added. The solution was then transferred into a Teflon-lined autoclave and heated at 80 °C for 3 h. The N-GHS were collected with centrifugation, followed by washing with deionized water several times.[23]

Characterization

High-resolution transmission electron microscopy (HRTEM) using a JEOL operated at an accelerating voltage of 200 kV. Powder X-ray diffraction (XRD) patterns were measured with a Bruker diffractometer, with Ni-filtered Cu Kα radiation (λ = 1.5418 Å). Raman spectra were recorded on a Jobin-Yvon Triax 550 spectrometer (1200 grooves per mm), using the 514.5 nm (2.41 eV) line of an Ar ion laser (power = 0.3 mW) as the excitation source. Optical characteristics were recorded on a Cary 5000 Ultra Violet-Visible-Near Infrared (UV/Vis/NIR), spectrophotometer and a Perkin Elmer LS 55 fluorescence spectrometer. Quantum yields (QYs) were calculated by the comparative "gradient method". The nanosecond Nd-YAG laser (BMI, 10 Hz, 7 ns) laser was utilized as an excitation source for the time-resolved photoluminescence. The photoluminescence signal was collected at the perpendicular angle to the excitation beam and detected with a monochromator (Acton research, Spectro-275) and PMT (Hamamatsu, R928). The signal was acquired by 500 MHz digital oscilloscope (HP, 54520A) and transferred to a computer for data analysis. The surface charge (zeta potential) of GHS was determined by a zeta potentiometer (Malvern Instrument Zeta Potentiometer 3000). X-ray photoelectron spectroscopy (XPS) was acquired using an ESCALab 220i-XL spectrometer (Thermo VG, UK) with Al Kα radiation in twin anodes.

Cell-imaging and cytotoxicity experiment

The human cervical adenocarcinoma HeLa cells (2×10^4 cells) grown on coverslips were incubated with 200 μg mL^{-1} nanoparticles for 2 h. The cells were washed several times with ice-cold phosphate-buffered saline (PBS), fixed by incubation with freshly made 3% formaldehyde (containing 1.5% methanol) in PBS (pH 7.4) for 15 minutes, and neutralized with 50 mM NH_4Cl solution. After washing, the cells were visualized by fluorescence microscopy using an Axioplan Zeiss microscope and photographed with a digital camera (CCD). For Laser Scanning Confocal Microscopy (LSCM), the cells were visualized using a Zeiss LSM 510 confocal microscope (Nikon, Japan) equipped with Argon (488 nm) and HeNe (543 nm) lasers for fluorescence.

Cytotoxicity was assessed by measuring effects of GHS on cell proliferation and membrane damage, respectively. The effect of the GHS on cell proliferation was determined by WST-1 assay (Roche). Cells (2×10^3 cells per 100 μL) were seeded onto 96-well plates and incubated overnight at 37 °C under a 5% CO_2 atmosphere. The medium in the wells was then replaced with fresh medium containing GHS (1–1000 μg mL^{-1}) and incubation continued for 72 h. Briefly, 10 μL of WST-1 solution (Roche) was added to each well and the plates were further incubated. After 4 h, the absorbance was measured with a plate reader at 440 nm. Cells incubated without GHS were used as a control. The release of lactate dehydrogenase (LDH) was monitored with the CytoTox 96 Non-Radioactive Cytotoxicity Assay (Promega). Cells (2×10^4 cells per mL) grown on 24-well plates were incubated with GHS (0.5–1000 μg mL^{-1}) for 72 h. The plates were centrifuged, and aliquots (50 μL) of cell culture medium were collected from each well and placed in new microtiter plates.

Finally, 50 μL of substrate solution was added to each well and the plates were further incubated for 30 min at room temperature. The absorbance at 490 nm was measured with a microplate reader. Cytotoxicity is expressed relative to basal LDH release by untreated control cells. More detailed experimental conditions are described in the ESI.†

Statistical analysis was performed using Student's *t* test for unpaired data and *p* values of less than 0.05 were considered significant. All data were presented as mean ± standard deviation (SD).

Results and discussion

Fig. 1 shows a scheme of the synthetic route for the formation of GHS. In Step 1, we used a microemulsion method to coat Fe_3O_4 NPs (1) prepared from an iron oleate precursor, with uniform SiO_2 shells. This produced the Fe_3O_4@SiO_2 core–shell (2). Then under hydrothermal conditions, a graphite oxide coating was generated on Fe_3O_4@SiO_2 (2) by glucose carbonization. Deposition of the graphite oxide coating on Fe_3O_4@SiO_2 (2) from glucose happened along with core, *i.e.*, Fe_3O_4, elimination, resulting in SiO_2@GHS (3). By reducing the reaction time Fe_3O_4 cores can remain to yield Fe_3O_4@SiO_2@GHS. We removed the silica nano-templates in HF solution to produce GHS (4) or Fe_3O_4@GHS with an outer diameter of approximately 35 nm and a void size of ~20 nm (Fig. 2). The dispersibility in aqueous solution results due to the presence of functionalized surface oxygen groups on the GHS surface during the hydrothermal reaction with glucose. We confirmed the oxidized nature of the GHS (4) upon heating by elemental analysis (EA), which indicated C/O ratios of 2.10 and 2.34 for as-prepared and heat treated (4). These results are comparable with the C/O ratios of 1.8–2.5 observed in oxidized graphite by Szabo *et al.*[24] In Fig. 2(a), HRTEM shows the discrete Fe_3O_4 NPs with uniform size of ~8 nm. The silica coated magnetite spheres of Fe_3O_4@SiO_2 (2) were uniform in size, with an average particle diameter of ~25 nm. The GHS (4) form after the etching of SiO_2@GHS (3) in a highly concentrated HF solution to remove the silica residues. During the hydrothermal glucose carbonization on Fe_3O_4@SiO_2 (2), the size of the spherical Fe_3O_4 cores gradually decreased with an increase in reaction time (0–16 h) and finally the core disappeared, leaving vacancies (~20 nm) behind (Fig. 2(b)). The each of SAED patterns labeled corresponding crystal planes, shown in Fig. S1(a).† To confirm the disappearance of Fe_3O_4 cores during the reaction, we carried out Energy-dispersive X-ray analysis (EDX) (Fig. S1(b) and (c)†) and SQUID magnetic measurements (Fig. S1(d)†). Reduction of the magnetism of samples during the reaction indicating that magnetic core dissolved in samples. In addition, thickness of wall of resultant, GHS was ~10 nm, however the thickness could be controlled by reaction time (1–10 nm). HRTEM image of GHS labeled interlayer distances shown in Fig. S2,† indicating that interlayer distance of inner layers (0.34 nm) is shorter than that of outer layers (0.38 to 0.40 nm). Flat dense layers stacking observed inside of GHS, however, rough irregular stacking of layers in outside. In addition, according to report of Sun and Li,[7] growth of carbon nano-material derived from glucose under hydrothermal reaction described by the LaMer model.[25] In the carbonization process, hydrophobic layers were formed inside carbon spheres *via* dehydration and aromatization and hydrophilic layers are remained in outside. Based on this observation and report, GHS consisted of hydrophobic voids covered by hydrophilic oxidized graphite surfaces. It seems that the decomposed products of glucose during hydrothermal reaction are responsible for void formation in Fe_3O_4@SiO_2@GHS by dissolution of the core Fe_3O_4 particles and the slow dissolution process responsible for the well-dispersible colloidal particles. Under hydrothermal conditions, glucose undergoes intermolecular dehydration leading to aromatization and carbonization and also some decomposes to yield several acids[26] and the pH falls to 2–3. Thus magnetite dissolves slowly in present of glucose under hydrothermal conditions forming SiO_2@GHS. Zeta-potential analyses indicated that the surfaces of the GHS were negatively charged and GHS can readily form stable colloids without the need for either polymeric or surfactant stabilizers in a pH range between 4 and 11 (see ESI, Fig. S3†).

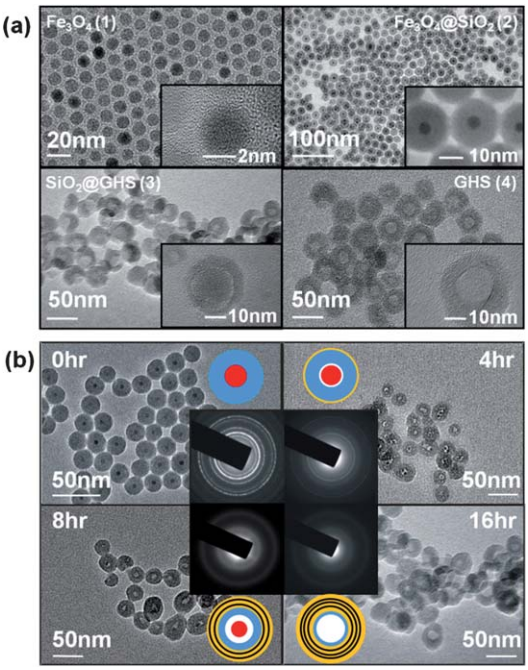

Fig. 2 (a) HRTEM images of monodisperse Fe_3O_4 NPs (1), Fe_3O_4@SiO_2 (2), SiO_2@GHS (3) and GHS (4). Insets show enlarged images of particles. (b) Time-dependant void formation in Fe_3O_4@SiO_2@GHS during hydrothermal graphite deposition reaction from glucose on Fe_3O_4@SiO_2 (2), as monitored by using HRTEM/SAED. Colors: magnetite – red, silica – blue, empty space – white, and graphite – orange.

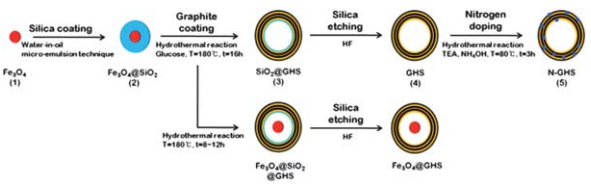

Fig. 1 Synthetic route for the formation of GHS.

The core–shell architecture Fe_3O_4@SiO_2 seems to offer special advantages as a template for forming uniform nano-sized multilayer carbon hollow spheres. The reactions lacking such a core–shell template produce either a large or featureless agglomerated carbon phase. For example, when Fe_3O_4 NPs without a SiO_2 coating were used as a template for carbonization from glucose, only carbon aggregates with multi Fe_3O_4 cores were obtained.[8–10] When silica balls without a Fe_3O_4 core were used as a template for carbonization by the hydrothermal method, the lumps of carbon embedded with many silica balls are obtained, as cited in the literature.[11] Since the yellow brown solution of GHS (4) exhibited noticeable fluorescence, we investigated the spectroscopic characteristics. We also synthesized N-GHS by hydrothermal reaction[23] to investigate effect of nitrogen doping on photoluminescence properties.

The powder-XRD pattern of GHS after heating at 450 °C in Ar atmosphere (see ESI S4†) shows the clear peaks of the graphite crystalline phases. The calculated unit cell parameters from powder-XRD of the hexagonal graphite lattice were $a = 2.91$ Å and $c = 7.16$ Å. The c parameter indicates that the interlayer distance of graphitic hollow spheres is longer than that of natural flat graphite flake, *i.e.* $c = 6.71$ Å. The longer layer distance of oxidized graphite hollow seems due to the curvature of sphere and functionalized oxygen groups on the graphite layers.

Raman spectra of GHS (4) and N-GHS (5) allowed an investigation of bonding features in the graphitic spheres (Fig. 3(a)). It was observed that both the GHS (4) and N-GHS (5) have a similar G bands, indicating the presence of the sp^2 carbon network and intensive defect-induced D bands of typical layered carbonaceous materials: 1338 cm^{-1} (D), 1595 cm^{-1} (G) for GHS (4) and 1340 cm^{-1} (D), 1591 cm^{-1} (G) for N-GHS (5). It was observed that both samples show broadening of the D band and high intensity ratio of D to G bands (2.6 for GHS (4) and 3.7 for N-GHS (5)). This indicates that there is enhancement of local distortion in N-GHS (5), probably due to sp^3 bonding from sp^2 bonding of graphite plane and also structural defects and edge plane exposure caused by heterogeneous nitrogen atom incorporation into the oxidized graphite layers. There is a previous report that N doping is very effective in introducing defects into the structure of carbon materials, it is manifested that the D band upshifts and its intensity increases while G band downshifts and the shifts are enhanced with the increase in the N/C atomic ratios of N-doped carbon materials.[27]

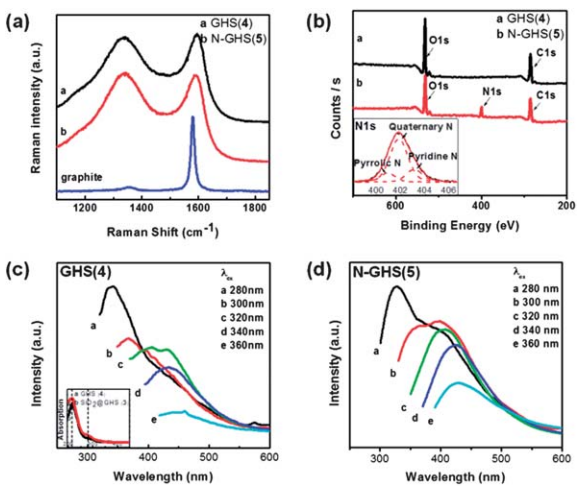

Fig. 3 (a) Raman spectra of GHS (4), N-GHS (5) and natural graphite flakes. Laser wavelength 514.532 nm (Ar-ion laser), power = 0.3 mW. (b) XPS spectra of GHS (4) (black line) and the N-GHS (5) (red line). Inset: XPS N 1s spectrum of the N-GHS. The N 1s peak can be split to three Lorentzian peaks at 400.6, 401.7 and 403.0 eV. (c) PL emission spectra at the room temperature for water dispersion of GHS (4). Inset: diffuse reflectance spectra of the GHS (4) (red line) and SiO_2@GHS (3) (black line). (d) PL emission spectra at the room temperature for water dispersion of N-GHS (5). The excitation wavelength of 280–360 nm were applied at the interval of 20 nm.

Fig. 3(b) shows the full-range XPS spectra and selected range N1s spectra. Only carbon, oxygen, and nitrogen species are detected in N-GHS (5) and the resultant N/C and C/O atomic ratio were calculated to be 0.18 and 2.17, respectively. These atomic ratios are comparable to those obtained from elemental analysis (EA). We also carried out EA, which indicated N/C and C/O ratios of 0.14 and 2.28, respectively. The survey scan of N-GHS reveals a main peak at 284.5 eV which is responsible for the binding energy of sp^2 graphitic C1s and additional peaks at 402 eV and 532 eV which are assigned to the binding energy of the N1s and O1s, respectively. The Gaussian multi-peak fit for each plot reveals that the N1s spectra consist of three strong peaks at 400.6, 401.7 and 403.0 eV. We believe that the peak at 400.6 eV attributed to the nitrogen atoms in pyrrolic or amine moieties; the peak at 401.7 eV attributed to quaternary or protonated nitrogen; the peak at 403.0 eV attributed to the nitrogen atoms in pyridine-N oxides.[23] These results indicate that N-GHS prepared by hydrothermal treatment is graphitic nitro-oxide. The photoluminescence spectra of GHS (4) (Fig. 3(c)) are rather broad and their emissions are excitation wavelength dependent. Variation in the excitation wavelength between 280 nm and 360 nm led to the emission maximum from 340 nm to 460. We also observed fluorescent microscopy images of GHS (4) (Fig. S5†). Absorbance measurements of SiO_2@GHS (3) and GHS (4) show the maximum absorbance at 220 nm with a shoulder around 280 nm (Fig. 3(c) inset). The absorbance peak at around 220 nm attributed to π–π^* transitions of C=C, and a shoulder around 280 nm attributed to n–π^* transitions of C=O in SiO_2@GHS (3) and GHS (4).[28] PL excitation spectrum of GHS (4) shows in ESI (Fig. S6†).

It has been reported that excitation dependent PL in layered carbon systems is a consequence of isolated sp^2 cluster with localized electron–hole (e–h) pairs in sp^3 oxidized carbon plane matrix.[12–15] In the graphene oxide layer, large fraction of carbon is sp^3 hybridized with oxygen in form of epoxy and hydroxyl group. Since the band gap between the π and π^* states generally depends on the size, shape, and fraction of the sp^2-domains, tunable PL emission can be achieved by controlling the nature of sp^2-sites. In our case, the surface of oxidized graphitic spheres GHS (4) might have locally varying fractions of sp^2 and sp^3 domains. At the same time, in the emission spectrum of N-GHS (5) emissions show similar variation of emission maximum, except for slightly blue shift comparing to GHS (4) (Fig. 3(d)). These observations demonstrate that variation of

nitrogen doping can tune band gap of π and π^* states in graphitic materials, thus PL emission also can be tunable. Previously, the band gap modulation of N-doped graphenes and their electronic properties were investigated.[29,30]

To estimate the fluorescence QY of GHS, we employed a comparative method with known QYs.[31] The reference compound, L-Tryptophan with a QY = 14%, was chosen to provide a good match with the spectral absorption and emission features of the test samples. A preliminary estimate put the QY of GHS (4) at 0.35 ± 0.03%.

Since GHS and N-GHS have intrinsic PL properties and water dispensability, they can be a potential candidate for cellular imaging or as drug delivery carriers. To test their cell-penetration capacity, cellular uptake experiments were performed by incubating HeLa cells with 200 μg mL^{-1} GHS and N-GHS for 2 h. Confocal microscopy images demonstrated that both GHS and N-GHS were internalized into cells and localized mainly in the cytoplasm (Fig. 4). The cells demonstrated blue, green and red fluorescence with the highest intensity in the blue region. Meanwhile, red fluorescence intensity was very faint, which is consistent with the photoluminescence spectra of GHS and N-GHS (Fig. 3(c) and (d)). It is important to note that N-doping did not affect cellular uptake behaviors of GHS. This result indicates that GHS and N-GHS are easily taken up by cells can be used as effective dual-colored biomarkers, thereby suggesting its great potential for biological and medical applications. Since the cores of Fe_3O_4 could be completely or partly eliminated in a controllable way, it can be used as a magnetic resonance imaging agent also. In addition, their easily modifiable hydrophilic surfaces for multi-functionality and hydrophobic voids covered by oxidized graphite make them promising candidates for applications in cellular photo-imaging and targeted drug delivery.

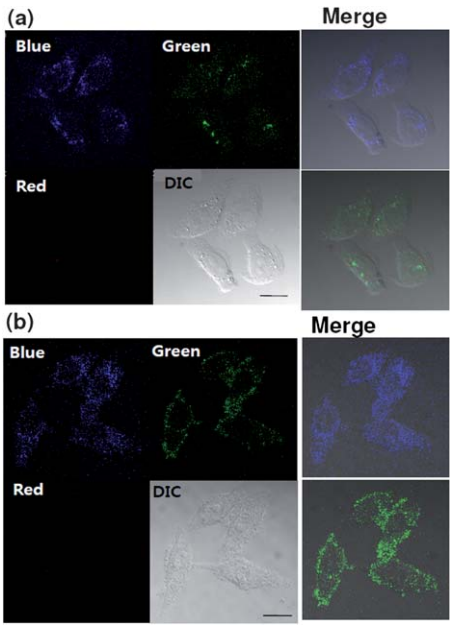

Fig. 4 Confocal microscopy images of HeLa cells incubated with GHS (a) and N-GHS (b), showing a high intensity of blue and green fluorescence in the cytoplasm. Scale bar and DIC represent 20 μm and differential interference contrast, respectively. Merged images of blue or green fluorescence with DIC in (a) and (b) clearly demonstrate the localization of both GHS and N-GHS in the cytoplasm.

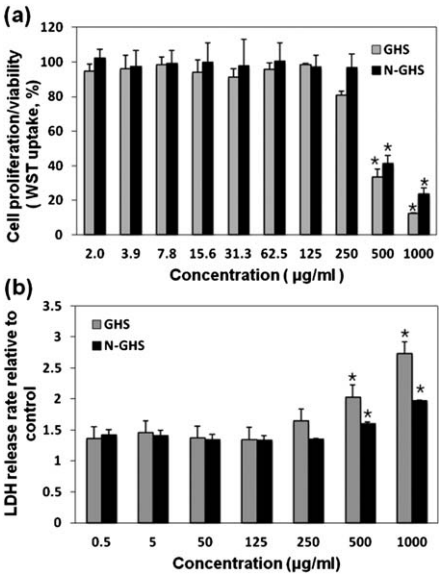

Fig. 5 (a) Effect of GHS and N-GHS on cell proliferation/viability of HeLa cell after 72 h incubation. (b) LDH release from HeLa cells treated with different concentrations of GHS and N-GHS for 72 h. * significant difference from the control group ($p < 0.05$).

The effects of GHS and N-GHS on cell proliferation/viability and membrane damage were evaluated in HeLa cells. Both GHS and N-GHS significantly inhibited cell proliferation/viability at high concentration of 500–1000 μg mL^{-1}, but did not affect cell proliferation up to 250 μg mL^{-1} (Fig. 5(a)). The WST-1 assay utilizes the tetrazolium salts which are cleaved to water soluble formazan by a cellular reduction mechanism, thus the amount of produced formazan is dependent on the number of metabolically active cells. On the other hand, the same result was obtained by LDH leakage assay, showing significant membrane damage in the cells treated with 500–1000 μg mL^{-1} (Fig. 5(b)). LDH is a cytosolic enzyme in normal cells, but released into the extracellular medium in damaged cells, so an increased LDH level in the medium is an indication of cell membrane damage. Interestingly, N-GHS had low effects on cell proliferation/viability and LDH release compared to GHS, suggesting that N-doping could reduce cytotoxicity of GHS. It is worth noting here that practical concentration levels applied for cell imaging and drug delivery are far less than 250 μg mL^{-1}. These results clearly suggest that GHS and N-GHS exhibited low toxicity, implying their great potential for biological and pharmaceutical applications.

Conclusions

Graphitic and N-doped graphitic hollow spheres were synthesized under hydrothermal conditions by a template method using double-shell composite Fe_3O_4@SiO_2 as a template. This low-temperature soft-chemical route will lead to further development of a new class of highly graphitized water-dispersible nanostructured materials. Cellular uptake experiment results

for GHS and N-GHS demonstrated their main localization in the cytoplasm and fluorescence signals in the cell. In addition, cytotoxicity tests revealed that GHS and N-GHS exhibited low toxicity in cells. Their rich surfaces with multiple functionalities, photoluminescence in the blue-green range, voids covered by multilayered graphite oxide, cell penetration capacity and low toxicity make them promising candidates for various biological and medical applications. The N-GHS reported here can extend into potential applications for drug delivery carrier. N-sites in N-GHS can provide anchoring sites for various metal complex species or electro-positive sites in drugs due to the lone pairs on N atoms.

Acknowledgements

This work was supported by the National Research Foundation of Korea (NRF) grant funded by the Korea government (MEST) (2012-0005186; 2012-0000650; 2012-000651; 2011-0017605). E.D. Grayfer acknowledges support from Russian Foundation for Basic Research, project 12-03-31502 mol_a. Y.-R. Kim thanks the support from the Pioneer Research Center Program through the National Research Foundation of Korea funded by the Ministry of Education, Science and Technology (No. 2012-0001066). H. Cheong acknowledges a grant (No. 2011-0031630) from the Center for Advanced Soft Electronics under the Global Frontier Research Program of MEST. S.-J. Choi thanks the support from a grant of the Korea Healthcare technology R&D Project, Ministry for Health, Welfare & Family Affairs, Republic of Korea (A085136). We are grateful to So Hyun Kim and Prof. Sungsu Park at Ewha Womans University for help in confocal imaging of GHS.

Notes and references

1 X. Chen, K. Kierzek, Z. Jiang, H. Chen, T. Tang, M. Wojtoniszak, R. J. Kalenczuk, P. K. Chu and E. Borowiak-Palen, *J. Phys. Chem. C*, 2011, **115**, 17717–17724.
2 C. Zhang, J. Li, E. Liu, C. He, C. Shi, X. Du, R. H. Hauge and N. Zhao, *Carbon*, 2012, **50**, 3513–3521.
3 Y. Han, X. Dong, C. Zhang and S. Liu, *J. Power Sources*, 2012, **211**, 92–96.
4 R.-T. Chiang, R.-K. Chiang and F.-S. Shieu, *Solid State Sci.*, 2012, **14**, 1221–1225.
5 R. J. White, K. Tauer, M. Antonietti and M.-M. Titirici, *J. Am. Chem. Soc.*, 2010, **132**, 17360–17363.
6 Y. Zhu, Y.-J. Bai, N. Lun, Y.-X. Qi, R. Liu and H.-L. Zhu, *Mater. Chem. Phys.*, 2012, **134**, 639–645.
7 X. Sun and Y. Li, *Angew. Chem., Int. Ed.*, 2004, **43**, 597–601.
8 X.-W. Wei, G.-X. Zhu, C.-J. Xia and Y. Ye, *Nanotechnology*, 2006, **17**, 4307–4311.
9 Z. Wang, H. Guo, Y. Yu and N. He, *J. Magn. Magn. Mater.*, 2006, **302**(2), 397–404.
10 S. Xuan, L. Hao, W. Jiang, X. Gong, Y. Hu and Z. Chen, *Nanotechnology*, 2007, **18**, 035602.
11 Y. Wan, Y.-L. Min and S.-H. Yu, *Langmuir*, 2008, **24**, 5024–5028.
12 Q. S. Mei, K. Zhang, G. J. Guan, B. H. Liu, S. H. Wang and Z. P. Zhang, *Chem. Commun.*, 2010, **46**, 7319–7321.
13 Z. Luo, P. M. Vora, E. J. Mele, A. T. C. Johnson and J. M. Kikkawa, *Appl. Phys. Lett.*, 2009, **94**, 111909.
14 F.-R. F. Fan, S. Park, Y. Zhu, R. S. Ruoff and A. J. Bard, *J. Am. Chem. Soc.*, 2009, **131**(3), 937–939.
15 G. Eda, Y.-Y. Lin, C. Mattevi, H. Yamaguchi, H.-A. Chen, I.-S. Chen, C.-W. Chen and M. Chhowalla, *Adv. Mater.*, 2010, **22**(4), 505–509.
16 Q.-L. Zhao, Z.-L. Zhang, B.-H. Huang, J. Peng, M. Zhang and D.-W. Pang, *Chem. Commun.*, 2008, 5116–5118.
17 S.-J. Yu, M.-W. Kang, H.-C. Chang, K.-M. Chen and Y.-C. Yu, *J. Am. Chem. Soc.*, 2005, **127**, 17604–17605.
18 Y. Wang, Y. Shao, D. W. Matson, J. Li and T. Lin, *ACS Nano*, 2010, **4**(4), 1790–1798.
19 Z.-S. Wu, W. Ren, L. Xu, F. Li and H.-M. Cheng, *ACS Nano*, 2011, **5**(7), 5463–5471.
20 H. M. Jeong, J. W. Lee, W. H. Shin, Y. J. Choi, H. J. Shin, J. K. Kang and J. W. Choi, *Nano Lett.*, 2011, **11**(6), 2472–2477.
21 L. Qu, Y. Liu, J.-B. Baek and L. Dai, *ACS Nano*, 2010, **4**(3), 1321–1326.
22 J. Park, K. An, Y. Hwang, J.-G. Park, H.-J. Hoh, J.-Y. Kim, J.-H. Park, N.-M. Hwang and T. Hyeon, *Nat. Mater.*, 2004, **3**(12), 891–895.
23 D. Long, W. Li, L. Ling, J. Miyawaki, I. Mochida and S.-H. Yoon, *Langmuir*, 2010, **26**(20), 16096–16102.
24 T. Szabo, O. Berkesi, P. Forgó, K. Josepovits, Y. Sanakis, D. Petridis and I. Dékány, *Chem. Mater.*, 2006, **18**, 2740–2749.
25 V. K. LaMer, *Ind. Eng. Chem.*, 1952, **44**, 1270.
26 D. Knežević, W. P. M. van Swaaij and S. R. A. Kersten, *Ind. Eng. Chem. Res.*, 2009, **48**(10), 4731–4743.
27 L. S. Panchakarla, K. S. Subrahmanyam, S. K. Saha, A. Govindaraj, H. R. Krishnamurthy, U. V. Waghmare and C. N. R. Rao, *Adv. Mater.*, 2009, **21**, 4726–4730.
28 Z. Luo, Y. Lu, L. A. Somers and A. T. C. Johnson, *J. Am. Chem. Soc.*, 2009, **131**, 898.
29 D. Wei, Y. Liu, Yu. Wang, H. Zhang, L. Huang and G. Yu, *Nano Lett.*, 2009, **9**(5), 1752–1758.
30 M. Deifallah, P. F. McMillan and F. Cor, *J. Phys. Chem. C*, 2008, **112**, 5447–5453.
31 Y. Liu, H. Wang, P. Liang and H.-Y. Zhang, *Angew. Chem., Int. Ed.*, 2004, **43**, 2690–2694.

